Probing the active sites of MoS₂ based hydrotreating catalysts using modulation excitation spectroscopy

Abhijeet Gaur[†,∥], Trine Marie Hartmann Dabros[‡], Martin Høj[‡], Alexey Boubnov[†#], Tim Prüssmann[∥], Jelena Jelic[∥], Felix Studt[†, ∥], Anker Degn Jensen[‡], Jan-Dierk Grunwaldt*[†,∥§]

[†]Institute for Chemical Technology and Polymer Chemistry, Karlsruhe Institute of Technology (KIT), Karlsruhe, D-76131 (Germany).

[‡]Department of Chemical and Biochemical Engineering, Technical University of Denmark (DTU), Kgs. Lyngby, DK-2800 (Denmark).

[∥]Institute of Catalysis Research and Technology, Karlsruhe Institute of Technology (KIT), Karlsruhe, D-76131 (Germany).

ABSTRACT: The reactive surface sites of MoS₂ hydrotreating catalysts (unpromoted as well as Co- and Ni-promoted) supported on MgAl₂O₄ spinel were investigated with respect to the substitution of sulfur by oxygen using *in-situ* XAS coupled with modulation excitation spectroscopy (MES). Specifically, MES experiments were carried out by periodically cycling between a H₂O and H₂S containing hydrogen gas mixture at 400 °C. Due to the low fraction of S-O exchange, conventional XANES and EXAFS data hardly showed any changes when these catalysts were exposed to increasing ratios of H₂O to H₂S in an H₂ atmosphere. XANES and EXAFS data extracted at the Mo K-edge by MES analysis showed that for approximately 1 % of the Mo atoms, sulfur atoms are replaced by oxygen atoms when exposed to H₂O, causing partial oxidation of these active sites. The reaction is reversible and Mo returns to its initial sulfide phase when H₂O is removed and H₂S is supplied in the feed. In case of Co- and Ni-promoted catalysts, the magnitude of S-O exchange was found to be reduced, indicating the beneficial effect of promotion. MES at the Ni K-edge showed that Ni was oxidized during H₂O exposure, which in turn delayed the Mo oxidation in the Ni-promoted catalyst. The structure of these catalysts under S-O exchange were modelled using density functional theory (DFT) calculations, showing that the edge atoms are affected strongly. For all three catalysts, OH substitution is more favorable, while O substitution could be possible at high H₂O pressure for unpromoted MoS₂. Mo K-edge XANES spectra calculated using these simulated structures support the results obtained from the MES experiments. The presented approach using MES in combination with XAS and supported by DFT can be extended in general to catalysts under *operando* conditions, and is thus a useful tool for determination of the active site on an atomic-scale.

KEYWORDS - X-ray absorption spectroscopy, Modulation excitation spectroscopy, Hydrotreating, Ni/Co-promoted MoS₂, Phase sensitive detection, S-O exchange

1. INTRODUCTION

Supported CoMo- and NiMo-sulfide catalysts are extensively used for hydrotreating of crude oil, primarily for the removal of sulfur.[1-5] While there is continued interest in the improvement of these catalysts due to ever increasing environmental regulations and the shift towards more sulfur containing feedstocks, these catalysts are also being investigated for the hydrotreating of feedstocks derived from biomass,[6-9] in particular bio-oil derived via fast pyrolysis. While the employment of these catalysts seems straightforward, there are some differences in the processes as well as in the process conditions. The shift towards bio-oil implies a shift from an oxygen poor (typically less than 0.3 wt%) to an oxygen rich feedstock (20 to 50 wt%)[10]. How this drastic change in oxygen chemical potential, which is also accompanied by a significantly lower shift of the sulfur content influences the stability and exact chemical composition of the active sites on the atomic-scale is still being vividly debated.[11-13]

Addressing this question is scientifically extremely challenging as the active sites of Co-MoS₂ and Ni-MoS₂ catalysts are believed to be located at the edges and corners of MoS₂, e.g. the sulfur edge in Ni-MoS₂ (see Figure 1), and thus only constitute a small fraction of all atoms in the catalyst. Studies using model catalysts with high edge concentrations revealed that MoS₂ single layers are predominantly terminated by the so-called Mo-edges and S-edges due to their lower edge-formation energies.[14-16] The atomic-scale structure and morphology of MoS₂, Co-MoS₂ and Ni-MoS₂ catalysts have been widely studied using density functional theory (DFT) along with transmission electronic microscopy (TEM) and scanning tunneling microscopy (STM).[17-18] DFT studies have indicated that exposure of MoS₂ to water vapor can lead to exchange of S with O at the active edge of MoS₂ and that promotion stabilizes the catalyst against these exchanges[19-20].

In the context of HDS, several studies have been published on CoMo and NiMo catalyst where reactivity of brim sites and

the influence of Co and Ni are reported.[17, 21-25] For the promoted MoS₂ hydrotreating catalysts, Co–Mo–S model suggest that the promoter atoms are located at edge positions of MoS₂ nanostructures and the substitution of Mo at edge sites enhance vacancy formation and the creation of active sites. Formation of promoted Co–Mo–S and Ni–Mo–S phases has been observed by distinct change in morphology compared to the unpromoted MoS₂ nanoclusters which exhibit a triangular crystal structure exposing only one type of edge. For model catalyst (on Au surfaces), a hexagonally truncated shape has been observed for nanocluster in Co–Mo–S where both Mo edges and S edges are present. In case of Ni–Mo–S, only larger clusters have a hexagonally truncated shape as the nature of the truncation depend on the cluster size. It has been suggested that Co and Ni promotion changes the electronic structure thereby modifying the brim states and lowers the S coordination on promoted edges causing adsorption of S-groups.

In order to adequately determine the structure and composition of the catalyst relevant for e.g. hydrodeoxygenation (HDO) of a bio-oil, characterization needs to take place under realistic reaction conditions. Common surface-sensitive spectroscopic techniques such as X-ray photoelectron spectroscopy (XPS)[26], Fourier-transform infrared (FTIR)[27] spectroscopy and Raman spectroscopy[28] have limitations due to broad signals, limited chemical specificity and operation at far-from-realistic reaction conditions. X-ray absorption spectroscopy (XAS), on the other hand, is element-specific and can probe the state of a catalyst under working conditions, owing to the high penetration of X-rays through reactor construction materials and the catalyst bed [29-31].
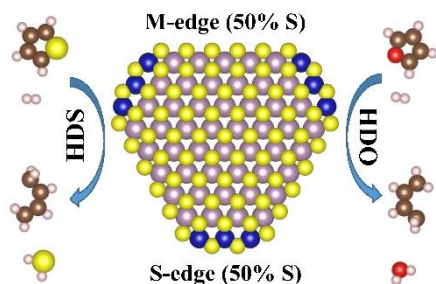

Figure 1. Simplified hexagonal model of a Ni-MoS₂ particle. Purple Mo, blue Ni, yellow S, red O, brown C and pink H. Schematics for role of Ni-MoS₂ in hydrodesulfurization (HDS) and hydrodeoxygenation (HDO).

The sensitivity of XAS towards minority species, however, is usually very low as it is probing the bulk. An enhancement of sensitivity has been achieved using high dispersion[32-33] or by placing atoms specifically on the surface[34-35]. Another elegant method is the application of transient experiments amplifying the response of some spectroscopic signals. One such method is modulation excitation spectroscopy (MES)[36] in which the catalytic system is modulated by periodically alternating between two externally applied conditions (e.g. concentration, reactants, temperature, pressure, pH) while the spectra are acquired continuously. MES is thus becoming more and more applied in conjunction with a number of time-resolved spectroscopic techniques such as XAS, X-ray diffraction (XRD), Raman, and IR[37-45]. Phase-resolved spectra extracted from an MES analysis exclusively provide signals from species responding to the external stimulation with the same frequency. This makes it possible to extract signals from minority species that are otherwise difficult to observe, if these species are responding to the changes

of the external conditions. MES is a strong method for resolving kinetics of multiple steps, e.g., in the case of a two-step reaction X → Y → Z, the characteristic signals of the different species will have maximum amplitudes at different phase angles and a thorough analysis can provide kinetic differentiation of pathways and lifetimes of active species during the modulation period.[43] In addition, the phase domain analysis could be used to yield quantitative kinetic information such as rate constants from the amplitudes and phase delays after back-transformation to the time domain.[43]

This technique thus provides an excellent tool to investigate the influence of the oxygen and sulfur concentration (and the variation hereof) on the specific atomic-scale composition and quantity of active sites and we will show herein how XAS-MES measurements supported by DFT calculations helped identifying the active sites of MoS₂, Co-MoS₂ and Ni-MoS₂ based catalyst as a function of the applied chemical potential. This study thus provides a detailed picture of the differences in active site composition at the atomic-scale between hydrodesulfurization (HDS) of crude oil and HDO of bio-oil.

2. EXPERIMENTAL

2.1 SULFIDATION SET-UP

MgAl₂O₄ supported MoS₂ (Mo, 3.4 wt% Mo), Ni-MoS₂ (NiMo, 2.8 wt% Mo), and Co-MoS₂ (CoMo, 3.3 wt% Mo) catalysts were prepared by sequential incipient wetness impregnation followed by calcination at 500 °C. The molar ratio of promotor (Ni and Co) to Mo was fixed at 0.3, to facilitate optimal hydroprocessing activity[1]. The loading of Mo was kept below 4 Mo atoms/nm² support surface area to facilitate spreading of the oxidic molybdate phase into a monolayer during calcination[46]. The MgAl₂O₄ support was chosen as a water tolerant alternative to γ-Al₂O₃, which is a dominant support for MoS₂ based catalysts[1, 47]. Details on the catalyst preparation and characterization composition was reported in previous work[48].
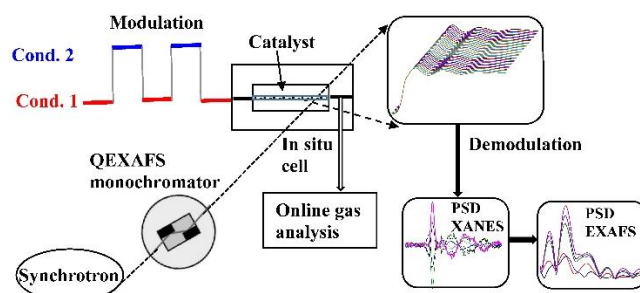

Figure 2. Experimental procedure employed for the MES experiments

Figure 2 shows the overview of the procedure employed for the MES experiments. Details of the setup for *in-situ* XAS measurements along with the process diagram are given in the ESI, figure S1. X-ray absorption near edge structure (XANES) as well as extended X-ray absorption fine edge structure (EXAFS) data were recorded simultaneously for each measurement. In the MES experiments, 6 mg catalyst was loaded into a 1-1.5 mm capillary. The oxide catalyst precursor was converted to the active sulfide form by treating it under a flow of 10% H₂S/H₂ (25-35 NmL/min) and heating to 400 °C with a holding time of 60 min at the target temperature. This in-situ sulfidation of oxidic

Mo, Co, and Ni precursors was monitored with XAFS, and the results have been reported in previous work[48]. During reaction, the sulfided sample was exposed to increasing ratios of H_2O/H_2S (30, 100, 190, and 300) in H_2 with a constant total flow rate of 43 NmL/min and a holding time of 30 minutes for each H_2O/H_2S ratio. Further details about these steady state experiments were reported in previous work[48].

For the MES experiments, a four-way valve was used to switch the flow to the capillary between H_2O/H_2 and H_2S/H_2. The time between switching the position of the valve was 3 minutes. In order to avoid pressure fluctuations, when switching between the two different gas flows, an adjustable check valve (V21 in Figure S1) was introduced downstream of the gas line keeping the pressure drop across the capillary and purge line almost equal (PI1 and PI2 in Figure S1). Catalysts were exposed to different molar ratios of H_2O/H_2S (30, 100, 190, and 300) corresponding to 100–500 ppm H_2S and 1.6–3.0% H_2O. From performed activity tests[48] full conversion corresponded to a H_2O/H_2S ratio of ≈125 and ≈30 at 550 and 2200 ppm H_2S, respectively. The ratios in the steady state experiments were chosen to fit 30 and 125, and then in the MES experiments it has been tried to go even higher to provoke the samples. Thus, MES studies were performed by cycling between 3% H_2O/H_2 (1st cycle, 180 seconds) and 1000 ppm H_2S/H_2 (2nd cycle, 180 seconds) with a total period of 360 seconds.

2.2 ACQUISITION OF QEXAFS DATA

Time-resolved quick-scanning EXAFS (QEXAFS)[49-50] spectra were collected at a frequency of 20 Hz for all samples at the Mo K-edge and for the NiMo sample also at the Ni K-edge. One MES experiment consisted of 10 periods of 6 minutes each making a total of 72,000 spectra. The recorded spectra were calibrated using a metal foil and then extracted in the form of $\mu(E)$ vs. E files using the JAQ code (version 3.3)[51]. To deal with the large amount of data, further analysis was performed using Matlab scripts. The extracted spectra were first normalized to edge position by fitting pre-edge and post-edge polynomials. After normalization, the spectra were averaged for obtaining the time resolved spectra. A set of 36 time-resolved spectra were obtained by averaging, each spectrum covering 10 seconds each that is additional merging groups of 200 scans of 0.05 second each. The averaging enhanced the signal-to-noise ratio for detection of small changes into a single 360-second period. These time resolved spectra are transformed into phase-resolved spectra using eq. 1, where the periodic changes occurring at identical phase shift during each period got added up thereby making it detectable.

$$\mu(E, \Delta\varphi) = \frac{2}{T} \int_0^T \mu(E, t) \sin\left(\frac{360°}{T} t + \Delta\phi\right) dt. \qquad (1)$$

The averaged time-resolved series of spectra $\mu(E, t)$ were demodulated[36, 52] into a phase-resolved set $\mu(E, \Delta\varphi)$, by probing it with a sine function of period T = 360 s and phase shift $\Delta\varphi$, $0° \leq \Delta\varphi < 360°$. The phase-resolved spectra were analyzed qualitatively and quantitatively by comparing them to difference spectra of pairs of compounds expected to result from the two alternating reaction conditions. In the present study, period wise analysis of the MES spectra was performed, i.e., initially only first period is taken and then consecutively other periods were added to the average. This step of observing phase resolved spectra by adding consecutive periods helps to confirm

that reversible phase changes occurred during all the periods which is an important criteria for applying MES analysis to any system.

X-ray absorption fine structure (XAFS) spectra were recorded at the SuperXAS beamline at the Swiss Light Source (SLS, Villigen, Switzerland). The storage ring was operated at 2.4 GeV with a ring current of 400 mA in top-up mode. The QEXAFS monochromator equipped with Si(111) and Si(311) channel-cut crystals was scanning at 10 Hz and spectra were recorded in transmission mode using fast, gridded ionization chambers capable of full-scan frequencies of up to 50 Hz[53]. Spectra were collected separately at the Ni K-edge (8333 eV), Co K-edge (7709 eV) and Mo K-edge (20,000 eV) for the catalysts under the same experimental conditions. For calibration and analysis purpose XAFS spectra of the reference compounds: MoO_3, MoO_2, CoS, CoO, Co_2O_3, Co_3O_4, Ni_3S_2, and NiO were also recorded.

2.3 XAFS DATA ANALYSIS

XANES as well as EXAFS spectra during steady state exposure to $H_2O/H_2S/H_2$ mixtures were obtained from averaging QEXAFS spectra recorded during the first 5 and the last 5 minutes of the total holding time, i.e., 30 minutes for each ratio. The EXAFS data analysis was performed using the software package IFEFFIT interfaces Athena and Artemis[54]. The recorded spectra were calibrated using a metal foil. The pre-processing of data includes background removal, normalizing with respect to the edge position and Fourier transformation (FT) of the resulting spectrum from k-space to R-space. Model structures obtained from references, i.e., sulfides and oxides of the corresponding metals, as well as simulated catalyst model structures have been used to fit the experimental data in R-space for determining the structural parameters. These parameters include energy shift of the path (ΔE_0), change in the half path length (ΔR), amplitude reduction factor (S_0^2), number of identical paths (N) and relative mean-square displacement of the atoms included in path (Debye-Waller factor, σ^2). Further details about the EXAFS data analysis are given in the ESI.

2.4 COMPUTATIONAL DETAILS (DFT)

DFT calculations were performed using the Vienna Ab Initio Simulation Package (VASP)[55-56] in connection with the Atomic Simulation Environment (ASE)[57] employing the Bayesian Error Estimation Functional with van der Waals correlations (BEEF-vdW)[58] The projector augmented wave method (PAW)[59-60] was used and the plane-wave cutoff energy was 500 eV. Infinite stripe models[61-62] consisting of a 4x4x1 super-cell and separated by more than 14 Å of vacuum space in the y and 20 Å in z directions were used to model the M-edge and S-edge for MoS_2 and Ni(/Co)-MoS_2. We performed additional DFT calculations on small MoS_2, $CoMoS_2$, $NiMoS_2$ clusters (appr. 2.4 nm in diameter) in order to validate the commonly used slab models[17, 19, 63] and find that the differences are rather small (see table S1 and figure S2). All atoms were allowed to relax during geometry optimizations with the convergence criterion set to a maximum force of 0.01 eV/Å. The Brillouin zone was sampled using a 2x1x1 Monkhorst–Pack k-point grid[64]. Spin polarization was considered for all calculations. On the already optimized structures, single point calculations were performed with the GGA+U method[65] in order to obtain more accurate binding energies. Values used are U = 3.5, 4.4, 5.0 eV for the Mo, Co and

Ni, respectively. Ab initio XANES calculations were performed using the DFT optimized model structures employing the FEFF9[66] code. More details can be found in the ESI.

3 RESULTS AND DISCUSSION

3.1 Active sulfide phase of Mo, CoMo and NiMo

Figure 3(a) shows the XANES spectra of the in-situ sulfided catalysts at 400 °C as compared to the reference MoS_2. It can be observed that features observed in the spectra of the catalysts are similar to that of MoS_2 indicating presence of MoS_2 phase in the samples. However, the intensity of these XANES features is quite low as compared to that in reference (high temperature effect). Figure 3(b) shows corresponding EXAFS spectra where amplitude of first peak, i.e., Mo-S peak is less than half than of its amplitude in reference. Very weak Mo-Mo contribution (second peak) has been observed in the higher shells.
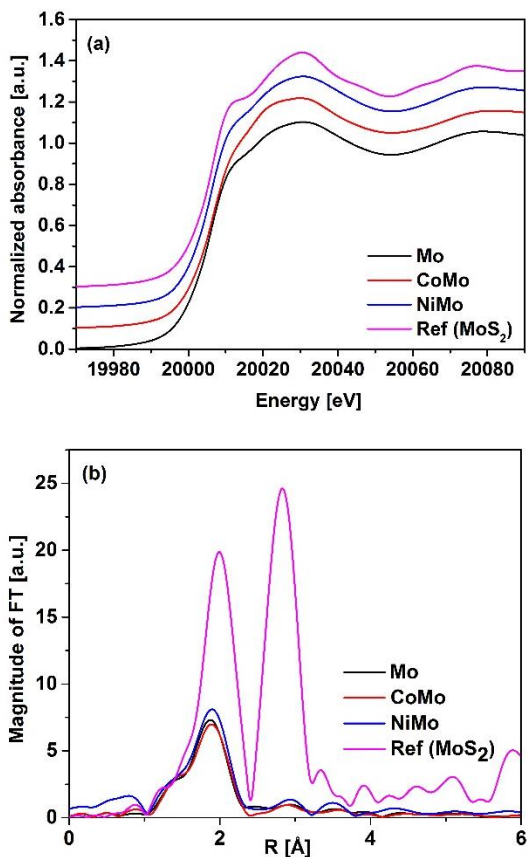

Figure 3. (a) Mo K-edge XANES spectra for in-situ sulfided catalysts at 400 °C prior to steady state and MES experiments. For comparison XANES spectrum of MoS_2 reference has also been presented. Spectra are displaced vertically for better presentation. (b) Corresponding Fourier transform spectra.

The details of the characterization of the sulfide phase prior to the steady state/MES experiment employing techniques of XAFS and TEM have been reported in previous work[48]. In case of sulfided NiMo catalyst (prepared as described herein) with 3.3 wt% Mo and a Ni/Mo molar ratio of 0.3, TEM results for particle size distribution based on >350 particles in >45 images showed that the majority of the sulfided phase was present as ~4 nm monolayer MoS_2-type slabs[48] (see figure S3). Structural parameters determined from fitting the Mo K-edge EXAFS

spectra of the sulfided catalysts at 400 °C and the reference MoS_2 are given in Tables S2-S4. For all the catalysts, Mo-S co-ordination at 2.40–2.41 Å with a CN of 4.1–4.8 (which is 6 in bulk phase) indicates presence of MoS_2 phase with sulfur deficient Mo sites which is in accordance with earlier studies[67-70]. Mo-Mo coordination at 3.16–3.17 Å is also in agreement with earlier reported values[67-68], however the values of CN=0.26–0.43 is too low. Note that these in-situ EXAFS measurements were conducted at high temperature which corresponds to the large Debye-Waller factor (thermal disorder) making EXAFS oscillations weaker and affecting the corresponding CNs[69]. Also, Mo atoms are present in thin flat slabs in these catalyst, thus CN will be 6 for the Mo atoms in the middle of the slabs but for those at the edges and corner it will be less and EXAFS measures the average of these CNs. It could be interesting to obtain detailed information on the particle morphology at model conditions by surface sensitive methods and compare it to scanning tunneling microscopy (STM) studies for model catalysts, such as MoS_2 on Au [17, 21, 71].

3.2 XANES and EXAFS during steady state exposure to H_2O/H_2S/H_2 mixtures.
3.2.1 Mo, CoMo, and NiMo at the Mo K-edge. Figure 4 displays XANES spectra of the Mo catalyst under different H_2O/H_2S ratios. Only small variations in the intensity of the shoulder H (inset) have been observed with changing ratios. Similarly, Fourier transformed (FT) EXAFS spectra given in the inset reveal only a small rise in the amplitude of the Mo-S and Mo-Mo peaks. Similarly, XANES and EXAFS spectra obtained at the Mo K-edge for the Co- and Ni-promoted catalysts hardly show any changes (see Figures S4-S6 and tables S2-S4).
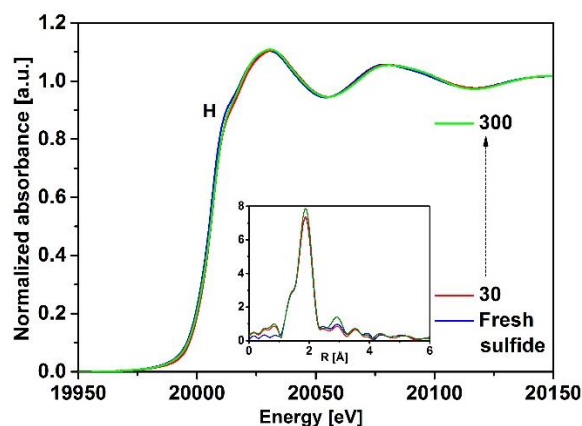

Figure 4. XANES spectra and as inset the corresponding FT spectra at the Mo K-edge for Mo (at 400 °C) under increasing H_2O/H_2S ratios (from 30 to 300, with 30 minutes exposure at each level). Shoulder H at 20008 eV is also shown.

Minor variations in the coordination number (CN) for the Mo-S shell at 2.40 Å suggests that the sulfide phase is stable under these varying H_2O/H_2S ratios. The Mo-Mo contribution was found at 3.16 Å with CN between 0.42 - 0.57.. Additionally, a Mo-O contribution at 1.62–1.65 Å with a very low CN of ~ 0.24 has been explained as interaction with the support[48], i.e. there is no actual bonding between Mo and O but only a slight interaction indicating formation of very small and highly dispersed MoS_2 particles. In the case of Co-MoS_2, Mo-Co contribution at 3.2 Å shows presence of Co on the surface of the catalyst. The CN of 4.3-4.6 for Mo-S suggests an increased sulfidation upon

Co-promotion. For Ni-MoS$_2$, the CN obtained for Mo-S in the sulfided phase is 4.8 with an average distance of 2.40 Å.

3.2.2 CoMo at the Co K-edge. Co K-edge XANES and FT EXAFS spectra for the CoMo sample under the different H$_2$O/H$_2$S ratios along with the EXAFS fitting results show that the metal-metal coordination found at ~ 3.8 Å for the sulfided sample at 400 °C indicate the presence of a Co$_9$S$_8$ phase (ESI, figure S4(c-d) and table S5). With changing H$_2$O/H$_2$S ratios this value shifts closer to the central Co atom, i.e. 3.2 Å, similar to that present in the CoMoS phase[72]. The Co-S CN first increases gradually with increasing ratio, reaching a maximum (3.1) at the end of exposure to the ratio of H$_2$O/H$_2$S = 100 and a minimum (2.1) at the end of ratio H$_2$O/H$_2$S = 300 showing an overall decrease in Co-S CN. However, in this case the corresponding measurement error in the CNs are also high. The initial increase in the CN of Co-S is possibly due to variation in proportions of Co$_9$S$_8$ and CoMoS phases under these conditions as suggested by experiments from Bouwens et al.[72] From figure S4(c-d), it can be concluded that there are changes which corresponds to transition between the CoMoS and Co$_9$S$_8$ phases but no indication of Co oxidation has been observed.

3.2.3 NiMo at the Ni K-edge. For the NiMo sample, Ni K-edge XANES and FT EXAFS spectra under the different H$_2$O/H$_2$S ratios along with the EXAFS fitting results confirms presence of metal-metal coordination of Ni-Ni at 2.8 Å and Ni-Mo at 3.3 Å, corresponding to the NiMoS phase[73] (ESI, figure S5 and table S6). The CN of Ni-S shows a slight decrease with increasing ratio until a H$_2$O/H$_2$S ratio of 190, but it increases again at the highest ratio of 300, reaching its initial value. Thus, the sulfided phase of Ni is stable under the increasing H$_2$O/H$_2$S ratios. From the results obtained by XAFS spectroscopy at the Mo, Co, and Ni K-edges it can be concluded that the metal contributions in higher shells were increased with increasing H$_2$O/H$_2$S ratios. However, the changes observed in XANES as well as EXAFS regions give no clear indication for the formation of oxide phases under the increasing concentration of H$_2$O. Earlier studies have indicated that exposure of MoS$_2$ to water vapor can lead to exchange of S with O at the active edge of MoS$_2$ and that promotion can stabilize the catalyst against these exchanges[19-20][74]. Due to the limitations of conventional XAFS spectroscopy such changes are difficult to observe as the proportion of metal atoms interacting with H$_2$O is rather low. We thus show the results of more sensitive MES measurements in the next section.

3.3 Modulation excitation XANES and EXAFS spectroscopy during H$_2$O/H$_2$ and H$_2$S/H$_2$ cycling

3.3.1 Dynamic changes over the Mo catalyst observed at 400°C at the Mo K-edge. Time-resolved XANES spectra obtained from 10 periods average into one period (a total of 36 spectra covering 10 seconds each) are shown in Figure 5(a) for the unpromoted Mo sample. The inset shows that the intensity of the shoulder H that is directly related to the Mo-S coordination remains mostly unaffected during cycling suggesting an intact sulfide phase of Mo. Since this is mainly the result of the low specificity of conventional XAS we investigated whether small atomic changes at the edges occurred by demodulating the time-resolved spectra into phase-resolved spectra. Figure

5(b) shows the demodulated spectra at selected values of phase shift (Δϕ) obtained from averaging the complete 10 periods measured for the Mo sample thus eliminating static features and achieving a high signal-to-noise ratio.
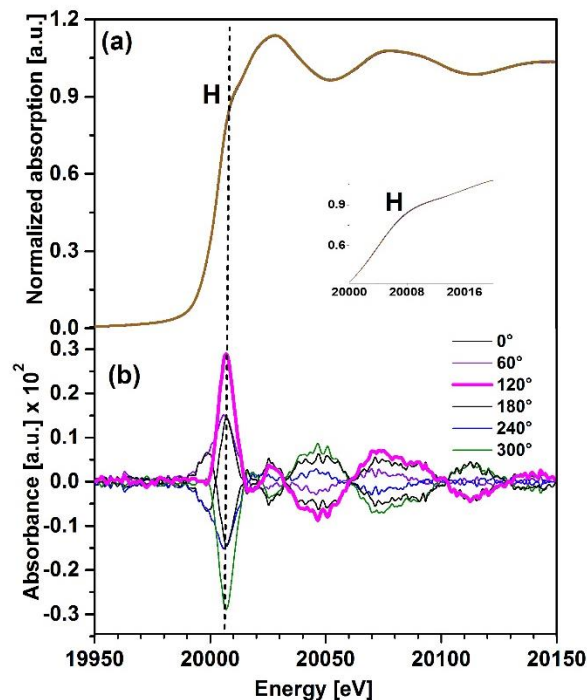

Figure 5. (a) Normalised time-resolved Mo K-edge XANES consisting of a total of 36 spectra covering 10 seconds each for the unpromoted Mo catalyst during 3 % H$_2$O/H$_2$ (0-180 s) vs. 1000 ppm H$_2$S/H$_2$ (180-360 s) cycling and 10 periods average. (b) Corresponding demodulated spectra at selected values of phase angle (Δϕ).

The features of the demodulated spectrum with the highest amplitude (phase shift Δφ = 120°) matched the difference between the spectra of the MoS$_2$ and MoO$_3$ references, as shown in Figure 6(a). Comparison of this standard difference spectrum with the demodulated spectrum obtained from MES (maximum amplitude) is shown in figure 6(b) revealing remarkable similarity. The amplitude of the demodulated spectrum was two orders of magnitude smaller than the difference of the reference spectra, corresponding to a reversible oxidation-sulfidation process for approximately one in every hundred Mo atoms. The kinetics of this process were obtained by tracking the absorption at 20,008 eV, the most dynamical spectral point and the position of the edge shoulder that has high adsorption for MoS$_2$, as a function of time as shown in Figure 7. The absorption steadily decreased during the H$_2$O cycle and increased during the H$_2$S cycle, best resembling the shape of the sine function with phase shift Δφ = 120°, as expected. The phase shift (Δφ) is the shift in the sine function that best follows the changes in the spectra. While the gas modulation follows a square wave in-phase with the sine function, the spectral response is slow and has a triangular wave resembling the cosine function, which is sine with a 90°-phase shift. We obtained maximal spectral changes at Δφ = 120°, which is close to the expected 90°.

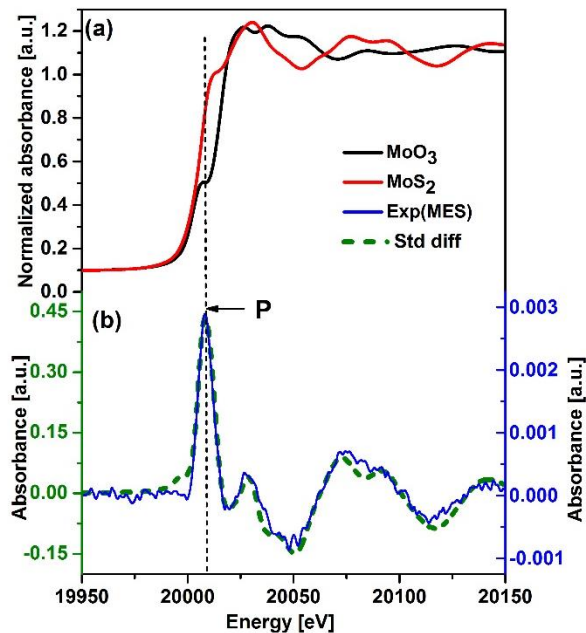Figure 6. (a) Experimental XANES spectra for MoS_2 and MoO_3, (b) Comparison of the (MoS_2 - MoO_3) difference spectrum (green dashed line) with the maximum amplitude signal obtained after demodulation (blue line) for the catalyst Mo.
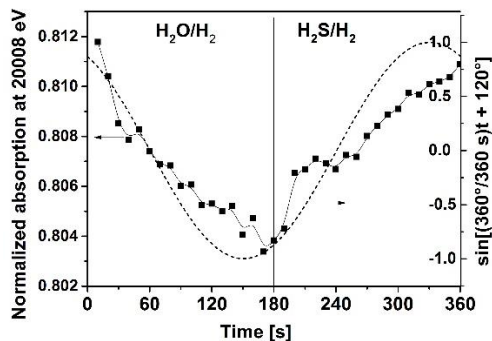

Figure 7. Kinetics of the phase transition of Mo observed using variation in intensity of the shoulder H at 20,008 eV as function of time. The dashed line is the Sine curve with a phase shift of 120°.

From the first period onwards, the demodulated spectra exhibit features similar to the difference spectrum of MoS_2 and MoO_3 as shown in ESI, Figure S7 which gives the demodulated spectra obtained by adding consecutive periods 1-9 to the average for the Mo catalyst. Addition of more periods to the average reduces the noise and enhances the signal showing that similar reactions are taking place during the two cycles of each period. In addition, the oxidation state changes from Mo^{4+} in the sulfide phase to Mo^{6+} in oxidized state and vice versa. This has been verified by looking at the features present in the difference spectrum of MoS_2 and MoO_2 which did not match with those obtained demodulated spectrum profile (see ESI, Figure S8), confirming that a change in oxidation state does indeed take place. The two difference spectra ($MoS_2 - MoO_3$) and ($MoS_2 - MoO_2$), are also compared to show the marked contrast between them.

Figure 8 shows the FT EXAFS spectrum obtained from demodulation (10 period average) for the Mo catalyst at phase angle

120°, at which a maximum amplitude is obtained and the corresponding k^3-weighted EXAFS spectrum is shown in the inset (demodulated EXAFS spectra for other selected phase angles are given in the ESI, Figure S9(a)). The first low amplitude peak at ~ 1.3 Å in the FT corresponds to the Mo-O coordination showing formation of Mo-O bonds during the first cycle (H_2O exposure). The second high amplitude peak at ~ 1.9 Å corresponds to the Mo-S coordination indicating that the Mo atoms underwent resulfidation during the second cycle (H_2S exposure). The third peak at ~ 2.9 Å is due to the Mo-Mo coordination that is mostly present in the sulfide phase.
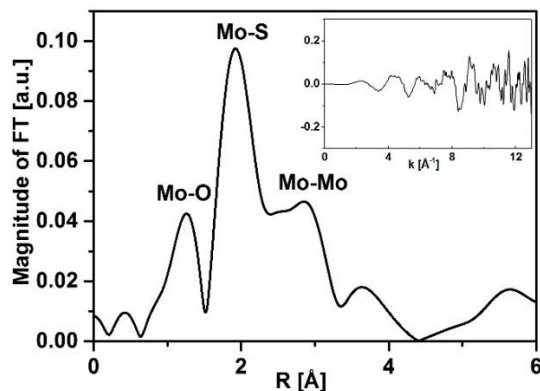

Figure 8. Fourier transformed spectrum at maximum amplitude, obtained after demodulation (10 periods average) at phase angle 120° at the Mo K-edge for the Mo catalyst. Inset shows corresponding demodulated k^3-weighted EXAFS spectrum.

EXAFS fitting results for this demodulated spectrum are given in table 1 and R-space fitting is given in ESI, figure S9 (b). Importantly, these phase-resolved spectra give only the signal of the spectral changes occurring during the experiment while features not undergoing changes are removed. Similar to the XANES spectrum, the amplitude of the phase resolved EXAFS spectrum is two orders of magnitude smaller compared to that of the reference spectra. Hence, all the obtained CN from the demodulated spectrum have been scaled by a factor of 10^2 for better comparison with the actual phases present in the catalyst. The Mo-O contribution was obtained at 1.73 Å which is close to the length of one of the Mo-O bonds in MoO_3 indicating formation of Mo-O bonds under the influence of H_2O. However, the obtained CN of the Mo-O shell (~1) is negative since demodulated spectra are difference spectra. From the demodulated EXAFS spectrum the Mo-S contribution was observed at 2.43 Å with a CN of 3.3 which is almost one less than the CN of 4 for the sulfide phase of this catalyst, as determined by standard EXAFS analysis in section 3.2.1. Hence, the total combined CN of Mo-O and Mo-S is still close to 4, indicating substitution of S with O.

Table 1. EXAFS fitting results for the maximum amplitude demodulated spectra at the Mo K-edge. S_0^2 was fixed to 1.0 as determined from the MoS_2. σ^2 for all the fitting paths were set to their standard value, i.e., 0.003±0.0006. χ_v^2 is the goodness-of-fit parameter.

Catalyst	Mo		NiMo		CoMo	
	R [Å]	CN ($\times 10^2$)	R [Å]	CN ($\times 10^2$)	R [Å]	CN ($\times 10^2$)

Mo-O	1.72	-1.2 ± 0.2	1.72	-1.3 ± 0.2	1.76	-0.9 ± 0.1
Mo-S	2.43	3.3 ± 0.2	2.41	2.7 ± 0.2	2.42	3.1 ± 0.2
Mo-Mo	3.17	2.3 ± 0.3	3.21	0.9 ± 0.4	3.21	1.1 ± 0.5
Mo-Ni / Mo-Co			3.25	1.8 ± 0.4	3.29	1.3 ± 0.5
	$\chi_v^2 = 1.6$		$\chi_v^2 = 0.89$		$\chi_v^2 = 1.3$	
	$\Delta E_0 = 1.8 \pm 0.3$		$\Delta E_0 = 2.8 \pm 1.8$		$\Delta E_0 = 4. \pm 0.5$	

In a separate experiment, the Mo catalyst at 450°C showed additional phase changes of Mo during similar cycling conditions as discussed in the ESI (figures S10-S14). Simultaneous reduction and oxidation of Mo was observed in this case showing that MES is a strong method for resolving multiple phase changes occurring in the system during transient conditions as the characteristic signals of the different species will have maximum amplitudes at different phase angles. The analysis of individual periods showed that different types of phase transitions took place, which are probably not reversible and, hence, conventional MES analysis cannot be performed in this case.

3.3.2 Effect of promotion – CoMo and NiMo catalysts at 400°C at the Mo K-edge. Figure 9 compares the maximum amplitude of the demodulated spectra obtained for CoMo and NiMo with Mo. The lower amplitude observed for CoMo and NiMo strongly suggests a decrease in S-O exchange upon promotion. The results obtained from MES analysis for the Co promoted catalyst look similar to those of the unpromoted catalyst (see Figures S15, S16 & S17). In this case, however, the demodulated spectrum has a maximum amplitude at phase shift $\Delta\varphi = 90°$ indicating different response compared to the unpromoted catalyst at 400 °C, where maximum amplitude was observed at $\Delta\varphi = 120°$ (see Section 3.2.1). Also, the amplitude at $\Delta\varphi = 90°$ for CoMo is comparatively lower than the amplitude at $\Delta\varphi = 120°$ for Mo showing that the level of S-O exchange decreased in the presence of Co, which is in agreement with the previous observations[20]. The variation in the absorption at 20,008 eV, shown in figure 10(a), is comparatively smaller but analogous to that of the unpromoted catalyst, also delayed by about 30 seconds, suggesting that the resulfidation of the Mo oxide phase has been delayed. For CoMo, EXAFS fitting results for the demodulated spectrum obtained at 90° are given in table 1, where Mo-O CN equal to ~1 indicate S being replaced by O. which is in accordance with the MES XANES results.
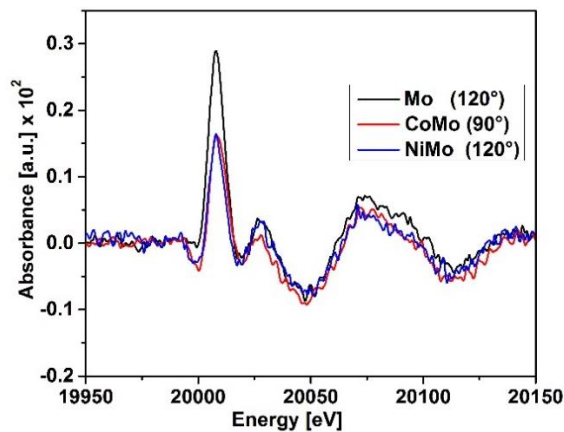

Figure 9. Comparison of the maximum amplitude signal obtained after demodulation for the three catalysts.

In case of NiMo, the phase resolved spectra at Mo K-edge showed almost no signal (only noise) during 1-4 cycles (ESI figures S18, S19 & S20). One of the possible explanation for such behavior may be that the Mo sites are not affected by these cycling conditions in the first four periods. However, as we proceed further with inclusion of the fifth period, phase resolved spectra starts giving signal indicating S-O exchange at Mo. The spectra show features similar to that of the difference spectrum MoS_2-MoO_3, indicating the formation of Mo-O bonds during the H_2O/H_2 cycle. From the sixth period and onwards the features in the demodulated spectra remain and the noise level decreased with inclusion of successive periods. These results indicate oxidation-resulfidation of Mo taking place during fifth to tenth period.
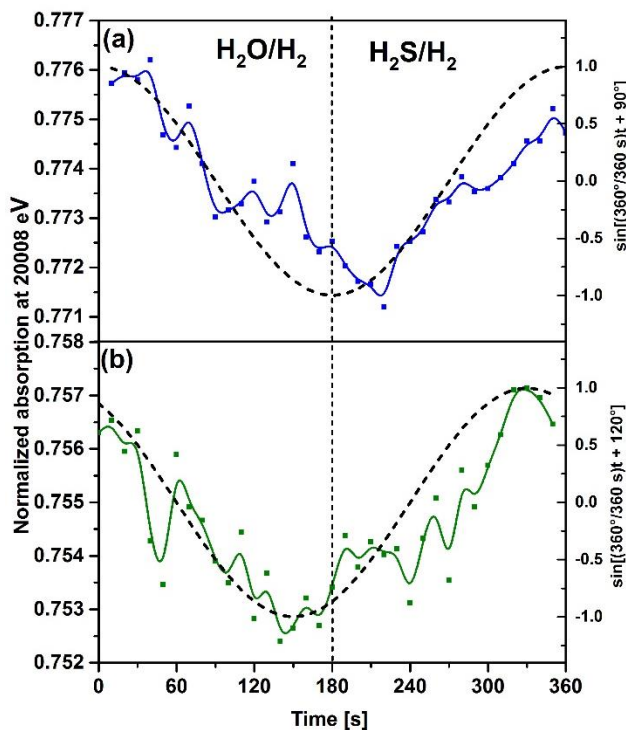

Figure 10. Variation in the intensity of shoulder H at 20,008 eV as function of time for (a) CoMo catalyst (the dashed line is the sine curve with a phase shift of 90°) and (b) NiMo catalyst (the dashed line is the sine curve with a phase shift of 120°).

7

For NiMo, the demodulated spectrum has a maximum amplitude at phase shift $\Delta\varphi = 120°$, which is similar to the value observed for Mo. Similar to CoMo, the amplitude for NiMo is comparatively lower than for Mo indicating a decrease in the S-O exchange. The variation obtained in the intensity of the peak at 20,008 eV are non-uniform as shown in figure 10(b), still the gradual decrease during the H_2O cycle and increased during the H_2S cycle has been observed. EXAFS fitting results for demodulated spectrum obtained at 120° are given in table 1 where Mo-O with CN of 1.3 (only magnitude) and Mo-S with CN of 2.7 has been observed showing the possible S-O exchange.

Note that the changes observed in the intensity of XANES features of phase resolved spectra are direct indicator of S-O exchange occurring during the cycling conditions. The intensity of XANES feature at 20008 eV decreases almost to half in case of CoMo and NiMo catalysts as compared to Mo clearly indicating weakening of this effect in the promoted catalysts. However, the amplitude of the demodulated spectrum was two orders of magnitude smaller than the difference of the reference spectra showing that these changes are quite weak and hence may not get completely transformed in the EXAFS part. The CNs obtained from EXAFS in the present study provide rather qualitative than quantitative information.

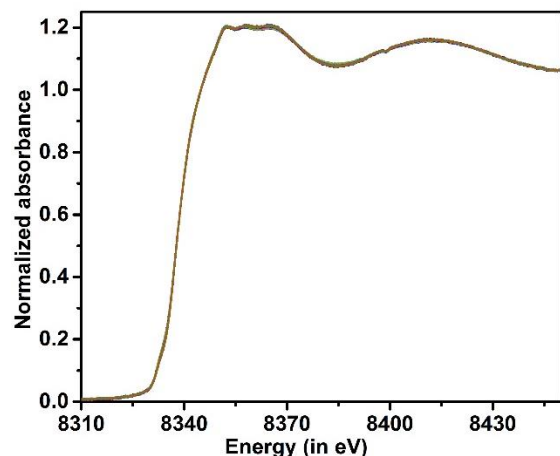*3.3.3 Dynamic changes at the Ni sites - NiMo catalyst at 400°C at the Ni K-edge.*

Figure 11. Average (10 periods) time-resolved XANES spectra of the sulfided NiMo at Ni K-edge consisting of a total of 36 spectra covering 10 seconds each during H_2O vs. H_2S cycling.

Figure 11 shows time-resolved XANES spectra of the sulfided NiMo catalyst at the Ni K-edge during H_2O vs. H_2S cycling obtained from averaging the complete 10 periods. Again no pronounced changes have been observed in characteristic features in these conventional spectra showing that Ni sulfide phase remains unaffected during cycling conditions. This indicate that the phase did not change significantly from that obtained by sulfidation at 400°C before the cycling, i.e. the NiMoS phase[48]. Corresponding demodulated XANES spectra of the sulfided NiMo catalyst at the Ni K-edge during H_2O vs. H_2S cycling, are shown in Figure 12(a) (For figures concerning the Ni K-edge MES analysis please see ESI, figures S21 and S22). Figure 12(b) shows the XANES spectra and the corresponding difference spectrum of the references Ni_3S_2 and NiO. The features observed in the demodulated spectra are not exactly the same as

the difference spectrum Ni_3S_2 − NiO. This may be due to the presence of a NiMoS phase instead of pure Ni sulfide after *in-situ* sulfidation. In addition, it cannot be claimed which Ni oxide species was formed during the cycling which may be a mixed Ni oxide phase. As the exact information about Ni phases appearing during the cycling conditions is not available, it is not possible to generate a difference spectrum similar to that obtained from phase resolved spectra. However, MES analysis can still be conducted with some characteristic features observed due to the presence of specific phase of an element. In the present case, the decrease in the white line due to the transformation from Ni oxide to Ni sulfide has been used as an indicator to show that Ni has been first oxidized and then resulfided during these conditions. The main negative peak Q in the difference spectrum at ~ 8347 eV, which corresponds to the presence of the intense white line in the Ni oxide spectrum, is observed in the demodulated spectra indicating oxidation of Ni during the first cycle (H_2O/H_2). Thus, MES XANES analysis shows that Ni is getting oxidized during the H_2O cycle.
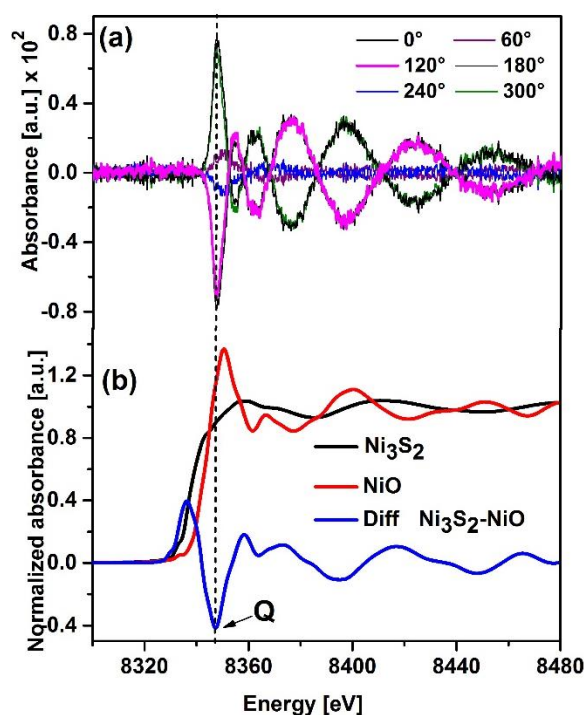

Figure 12. (a) . Demodulated XANES spectra at the Ni K-edge for the NiMo catalyst during H_2O vs. H_2S cycling. (b) XANES spectra for Ni_3S_2, NiO, and their corresponding difference spectrum. Feature Q is explained in the text.

Figure 13 shows the FT spectrum at 120° phase angle and the corresponding demodulated EXAFS spectrum is shown in the inset. Two overlapping peaks corresponding to Ni-O and Ni-S coordination are observed showing strong oxidation of Ni. From EXAFS fitting, Ni-O was observed at 2.07 Å with a CN of 6.0 (0.7) and Ni-S was found at 2.43 Å with a CN of 3.5(0.06) (CN scaled by factor of 10^2). σ^2 for all the fitting paths were set to their standard value, i.e., 0.003±0.0006. The value of χ_v^2 is 5.9 and ΔE_0 is 5.5± 0.4. Thus, in this case unlike Mo, there seems to be no S-O exchange over Ni as the CN of 6 for the Ni-O shell indicate formation of separate Ni oxide species, present in very low concentration. This large CN shows that some Ni atoms were completely oxidized during the first cycle of

8

H_2O/H_2. Additionally, during the H_2S/H_2 cycle, the Ni sulfide phase reappears with a CN of 3.5 for Ni-S which is similar to that of the NiMoS phase observed in the freshly sulfided catalyst. These CNs here present a trend and should be examined in future. The longer Ni-S distance 2.43 Å may be due to higher value of disorder at 400 °C.

Note that the oxidation of Ni is observed from the first period (ESI, figure S21) and thus faster than the S-O exchange at the Mo-edge where first detectable change was observed after five periods (Mo K-edge results of NiMo, Section 3.2.2). Figure 14 sketches the processes that take place on a Ni-MoS_2 particle: At high H_2S pressures, the M and S edge would primarily consist of S. With increasing H_2O pressure, fast interaction of oxygen from H_2O occurs at the Ni edge within the timeframe of our measurements. After 5 cycles we also observe the S-O exchange at the Mo-edge indicating that this interaction is kinetically slower.
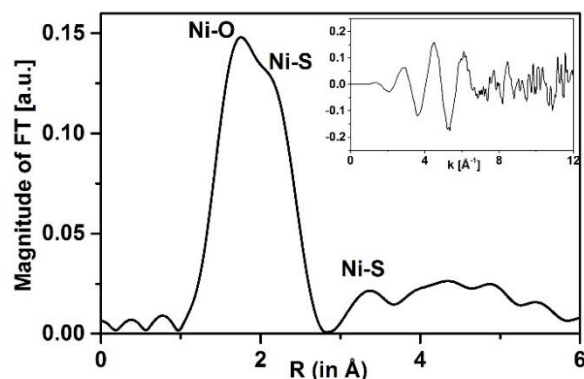

Figure 13. Fourier transformed spectrum for maximum amplitude signal obtained after demodulation (10 periods average) at phase angle 120° at the Ni K-edge for the NiMo catalyst. Inset shows corresponding k^2-weighted EXAFS spectrum.
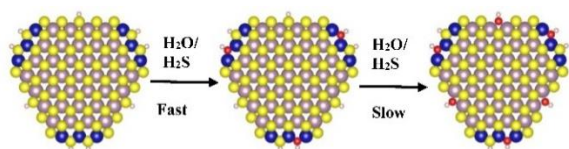

Figure 14. Schematic representation of the structural changes of the Ni-MoS_2 particles in two steps during the cyclic change towards a linked H_2O/H_2S ratio in the gas phase. Color scheme as in figure 1.

MES experiments were also performed at Co K-edge for the CoMo catalyst. However, due to low energy and high acquisition frequency, the spectral quality of the obtained data was not sufficient, also not with a different sample spot and capillary size. Some unexpected drift was observed during acquisition of the QEXAFS spectra making the analysis very challenging.

3.4 DFT calculations

3.4.1 DFT calculations of oxygen-sulfur exchanges. Models used for the DFT calculations performed in this study are similar to models reported in previous studies[17, 19-20, 63, 74] dealing with the particle sizes comparable to the ones obtained herein. The main objective of the DFT calculations was to define the stability of different terminations of M- and S-edges edges of

Ni(/Co)MoS_2 in the different H_2O, H_2S and H_2 gas phase environments. Structures were optimized for 50 % S coverage, for both the M-edge of the MoS_2 and the S-edge for Ni(/Co)-MoS_2, hydrogen terminated edges, S(H) vacancies as well as with O and OH adsorption (substitution) (see Table 2; optimized structures are given in ESI, figure S23). While vacancy formation of Co-MoS_2 is calculated to 0.41 eV, this value decreases for MoS_2 (0.18 eV) and is smallest for Ni-MoS_2 (-0.03 eV), indicating the possibility of vacancy formation for the latter two. The calculated OH and O substitution free energies decrease from CoMo to NiMo and are somewhere in between for the M-edges of MoS_2.

Table 2. Calculated free energies.[a]

(eV)	H	vacancy	OH	O
MoS_2 – M edge	-0.34	0.18	0.00	1.46
Co-MoS_2 – S egde	-0.29	0.41	0.26	1.78
Ni-MoS_2 – S egde	-0.81	-0.03	-0.25	1.34

(a) H – single H adsorption (25% H coverage); vacancy – energy of the vacancy formation as a reference to SH termination (25% H coverage for MoS_2 and Co-MoS_2 and 100% H coverage for Ni-MoS_2); OH – substitution energy referenced to SH termination, O – substitution energy referenced to SH termination. Conditions are T=400 °C, p(H_2) = p(H_2S) = p(H_2O) = 1 bar

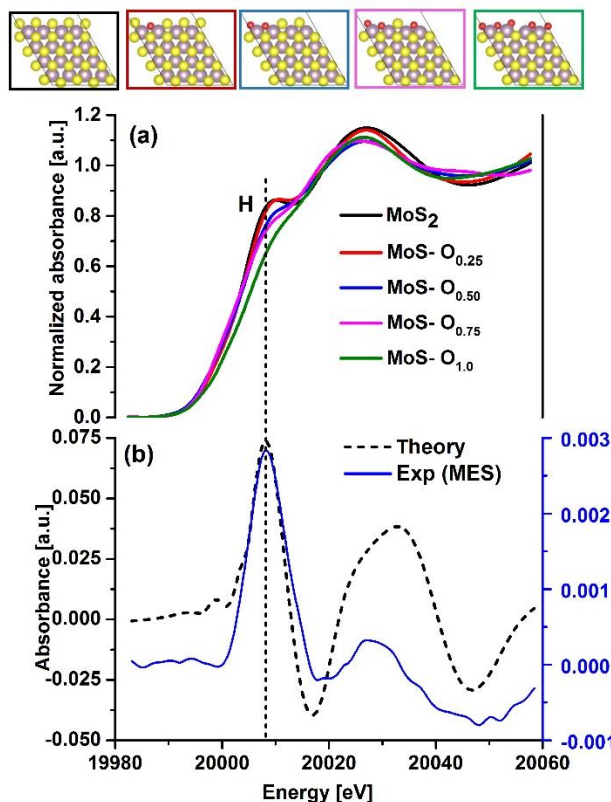*3.4.2 Calculated XANES spectra*

Figure 15 (a) Calculated Mo K-edge XANES spectra for the simulated MoS_2 structure and for O substitution equal to 0.25 (red), 0.50 (blue), 0.75 (pink) and 1.0 (green) on this MoS_2 structure. (b) Comparison of the obtained difference spectrum from these theoretical XANES spectra with the maximum amplitude signal shown in Figure 4b.

We simulated XANES spectra for the optimized DFT structures of MoS_2 where sulfur was replaced by oxygen at the edges. The spectra were simulated by averaging the core-holes in Mo atoms

at all possible positions on the surface to get the final spectrum. The simulated spectra are given in Figure 15(a) and the corresponding structures are shown on the top with identical colour codes. The intensity of the shoulder feature H decreases with S/O substitution (modeled here from 0.25 ML to 1ML) with the shoulder almost disappearing upon complete substitution. Thus, these simulated XANES spectra confirm that the intensity of the shoulder feature is directly related to the S/O atoms coordinated to Mo making variations of this feature a good parameter to indicate the level of S-O exchange. The theoretical difference spectrum for the fully sulfided and oxidized Mo-edge (obtained from merging spectra for all possible O substitutions from 0.25 to 1.0) is compared with the maximum amplitude demodulated spectrum obtained from MES analysis (Fig. 15(b)). The similarity between the theoretical and experimental spectra suggests that S atoms are replaced by O atoms during H_2O/H_2 and H_2S/H_2 cycling conditions.

4. CONCLUSION

By employing MES coupled XAS for unpromoted as well as Co- and Ni-promoted MoS_2 catalysts, we can conclude that upon cycling between H_2O/H_2 and H_2S/H_2 conditions, O atoms replace S atoms at the edges of MoS_2, the insight which is not accessible by conventional XAS. The results give important complementary insight to surface science studies for unraveling the mechanism and role of Mo-S and Mo-O during hydrodesulfurization and hydrodeoxygenation reactions. In the case of the Ni-promoted catalyst, MES-XAS measurements at the Ni K-edge revealed fast oxidation of the Ni-edge while the S-O exchange at the Mo-edge is rather slow. Theoretical calculations based on DFT confirmed the experimental observations and suggest that the thermodynamics of the S/O exchange become more favourable in the order Ni-edge > Mo-edge > Co-edge. Mo K-edge XANES spectra simulated from DFT optimized structures of MoS_2 and $MoS-O_x$ confirm the correlation between the XANES features observed in the phase resolved spectra and S-O exchange. Hence, by employing MES-XAS in conjunction with DFT, changes of the active sites of MoS_2-based catalysts could be detected at the atomic-scale.

In summary, we showed that by employing well-designed experiments MES is able to probe changes on catalyst surfaces at the atomic-scale as a function of variation in the chemical environment. The connection with X-rays further opens the possibility for high sensitivity *operando* measurements. Importantly, we also showed that kinetics of reaction occurring at the time scale of the MES measurements can also be probed.

ASSOCIATED CONTENT

Supporting Information. Process diagram of the in-situ EXAFS setup, DFT optimized clusters, TEM image for sufided NiMo, details on EXAFS data analysis and XAFS spectra during steady state, corresponding fitting results, period wise demodulated spectra for Mo, CoMo, NiMo at the Mo K-edge and for NiMo at the Ni K-edge obtained from MES analysis. MES results and discussion for the Mo catalyst at 450 °C. EXAFS fitting curves for maximum amplitude demodulated spectra for Mo, CoMo and NiMo. DFT optimized structures for 50 % S coverage, for both the M edge of the MoS_2 and the S edge of Ni(/Co)-MoS_2, hydrogen terminated edges, S(H) vacancies as well as with O and OH adsorption (substitution). This material is available free of charge via the Internet at http://pubs.acs.org.

AUTHOR INFORMATION

Corresponding Author

*Email grunwaldt@kit.edu

Present Addresses

*Institute of Catalysis Research and Technology, Karlsruhe Institute of Technology (KIT), Karlsruhe, D-76131 (Germany).
**Stanford Synchrotron Radiation Lightsource (SSRL), SLAC National Accelerator Laboratory, Menlo Park, CA 94025 (USA).

REFERENCES

(1) Topsøe, H.; Clausen, B. S.; Massoth, F. E. Hydrotreating Catalysis. In *Catal. Sci. Tech.*, Anderson, J. R.; Boudart, M., Eds.; Springer Berlin Heidelberg: Berlin, Heidelberg, 1996; pp 1-269.

(2) Wang, H.; Male, J.; Wang, Y. Recent Advances in Hydrotreating of Pyrolysis Bio-Oil and Its Oxygen-Containing Model Compounds. *ACS Catal.* **2013,** *3*, 1047-1070.

(3) Signorile, M.; Damin, A.; Budnyk, A.; Lamberti, C.; Puig-Molina, A.; Beato, P.; Bordiga, S. MoS_2 supported on P25 titania: A model system for the activation of a HDS catalyst. *J. Catal.* **2015,** *328*, 225-235.

(4) Castillo-Villalón, P.; Ramirez, J.; Castañeda, R. Relationship between the hydrodesulfurization of thiophene, dibenzothiophene, and 4,6-dimethyl dibenzothiophene and the local structure of Co in Co−Mo−S sites: Infrared study of adsorbed CO. *J. Catal.* **2012,** *294*, 54-62.

(5) Ferdous, D.; Dalai, A. K.; Adjaye, J. X-ray absorption near edge structure and X-ray photo electron spectroscopy analyses of $NiMo/Al_2O_3$ catalysts containing boron and phosphorus. *J. Mol. Catal. A: Chem.* **2005,** *234*, 169-179.

(6) Furimsky, E. Hydroprocessing challenges in biofuels production. *Catal. Today* **2013,** *217*, 13-56.

(7) Mortensen, P. M.; Grunwaldt, J.-D.; Jensen, P. A.; Knudsen, K. G.; Jensen, A. D. A review of catalytic upgrading of bio-oil to engine fuels. *Appl. Catal. A* **2011,** *407*, 1-19.

(8) Mortensen, P. M.; Grunwaldt, J.-D.; Jensen, P. A.; Jensen, A. D. Screening of Catalysts for Hydrodeoxygenation of Phenol as a Model Compound for Bio-oil. *ACS Catal.* **2013,** *3*, 1774-1785.

(9) Dabros, T. M. H.; Stummann, M. Z.; Høj, M.; Jensen, P. A.; Grunwaldt, J.-D.; Gabrielsen, J.; Mortensen, P. M.; Jensen, A. D. Transportation fuels from biomass fast pyrolysis, catalytic hydrodeoxygenation, and catalytic fast hydropyrolysis. *Prog. Energy Combust. Sci.* **2018,** *68*, 268-309.

(10) Oyebanji, J. A.; Okekunle, P. O.; Lasode, O. A.; Oyedepo, S. O. Chemical composition of bio-oils produced by fast pyrolysis of two energy biomass. *Biofuels* **2017,** 1-9.

(11) Likith, S. R. J.; Farberow, C. A.; Manna, S.; Abdulslam, A.; Stevanović, V.; Ruddy, D. A.; Schaidle, J. A.; Robichaud, D. J.; Ciobanu, C. V. Thermodynamic Stability of Molybdenum Oxycarbides Formed from Orthorhombic Mo_2C in Oxygen-Rich Environments. *J. Phys. Chem. C* **2018,** *122*, 1223-1233.

(12) Santosh, K. C.; Longo, R. C.; Wallace, R. M.; Cho, K. Surface oxidation energetics and kinetics on MoS_2 monolayer. *J. Appl. Phys.* **2015,** *117*, 135301.

(13) Yamamoto, M.; Einstein, T. L.; Fuhrer, M. S.; Cullen, W. G. Anisotropic Etching of Atomically Thin MoS_2. *J. Phys. Chem. C* **2013,** *117*, 25643-25649.

10

(14)Bollinger, M. V.; Jacobsen, K. W.; Nørskov, J. K. Atomic and electronic structure of MoS_2 nanoparticles. *Physical Review B* **2003**, *67*, 085410.

(15)Helveg, S.; Lauritsen, J. V.; Lægsgaard, E.; Stensgaard, I.; Nørskov, J. K.; Clausen, B. S.; Topsøe, H.; Besenbacher, F. Atomic-Scale Structure of Single-Layer MoS_2 Nanoclusters. *Phys. Rev. Lett.* **2000**, *84*, 951-954.

(16)Bollinger, M. V.; Lauritsen, J. V.; Jacobsen, K. W.; Nørskov, J. K.; Helveg, S.; Besenbacher, F. One-Dimensional Metallic Edge States in MoS_2. *Phys. Rev. Lett.* **2001**, *87*, 196803.

(17)Lauritsen, J. V.; Kibsgaard, J.; Olesen, G. H.; Moses, P. G.; Hinnemann, B.; Helveg, S.; Nørskov, J. K.; Clausen, B. S.; Topsøe, H.; Lægsgaard, E.; Besenbacher, F. Location and coordination of promoter atoms in Co- and Ni-promoted MoS_2-based hydrotreating catalysts. *J. Catal.* **2007**, *249*, 220-233.

(18)Lauritsen, J. V.; Besenbacher, F. Atom-resolved scanning tunneling microscopy investigations of molecular adsorption on MoS_2 and CoMoS hydrodesulfurization catalysts. *J. Catal.* **2015**, *328*, 49-58.

(19)Badawi, M.; Cristol, S.; Paul, J.-F.; Payen, E. DFT study of furan adsorption over stable molybdenum sulfide catalyst under HDO conditions. *C. R. Chim.* **2009**, *12*, 754-761.

(20)Badawi, M.; Paul, J. F.; Cristol, S.; Payen, E.; Romero, Y.; Richard, F.; Brunet, S.; Lambert, D.; Portier, X.; Popov, A.; Kondratieva, E.; Goupil, J. M.; El Fallah, J.; Gilson, J. P.; Mariey, L.; Travert, A.; Maugé, F. Effect of water on the stability of Mo and CoMo hydrodeoxygenation catalysts: A combined experimental and DFT study. *J. Catal.* **2011**, *282*, 155-164.

(21)Besenbacher, F.; Brorson, M.; Clausen, B. S.; Helveg, S.; Hinnemann, B.; Kibsgaard, J.; Lauritsen, J. V.; Moses, P. G.; Nørskov, J. K.; Topsøe, H. Recent STM, DFT and HAADF-STEM studies of sulfide-based hydrotreating catalysts: Insight into mechanistic, structural and particle size effects. *Catal. Today* **2008**, *130*, 86-96.

(22)Lauritsen, J. V.; Helveg, S.; Lægsgaard, E.; Stensgaard, I.; Clausen, B. S.; Topsøe, H.; Besenbacher, F. Atomic-Scale Structure of Co−Mo−S Nanoclusters in Hydrotreating Catalysts. *J. Catal.* **2001**, *197*, 1-5.

(23)Lauritsen, J. V.; Bollinger, M. V.; Lægsgaard, E.; Jacobsen, K. W.; Nørskov, J. K.; Clausen, B. S.; Topsøe, H.; Besenbacher, F. Atomic-scale insight into structure and morphology changes of MoS2 nanoclusters in hydrotreating catalysts. *Journal of Catalysis* **2004**, *221*, 510-522.

(24)Lauritsen, J. V.; Nyberg, M.; Vang, R. T.; Bollinger, M. V.; Clausen, B. S.; Topsøe, H.; Jacobsen, K. W.; Lægsgaard, E.; Nørskov, J. K.; Besenbacher, F. Chemistry of one-dimensional metallic edge states in MoS 2 nanoclusters. *Nanotechnology* **2003**, *14*, 385.

(25)Tuxen, A. K.; Füchtbauer, H. G.; Temel, B.; Hinnemann, B.; Topsøe, H.; Knudsen, K. G.; Besenbacher, F.; Lauritsen, J. V. Atomic-scale insight into adsorption of sterically hindered dibenzothiophenes on MoS2 and Co−Mo−S hydrotreating catalysts. *J. Catal.* **2012**, *295*, 146-154.

(26)Alayoglu, S.; Somorjai, G. A. Nanocatalysis II: In Situ Surface Probes of Nano-Catalysts and Correlative Structure−Reactivity Studies. *Catal. Lett.* **2015**, *145*, 249-271.

(27)Zaera, F. New advances in the use of infrared absorption spectroscopy for the characterization of heterogeneous catalytic reactions. *Chem. Soc. Rev.* **2014**, *43*, 7624-7663.

(28)Kim, H.; Kosuda, K. M.; Van Duyne, R. P.; Stair, P. C. Resonance Raman and surface- and tip-enhanced Raman spectroscopy methods to study solid catalysts and heterogeneous catalytic reactions. *Chem. Soc. Rev.* **2010**, *39*, 4820-4844.

(29)Grunwaldt, J.-D.; Caravati, M.; Hannemann, S.; Baiker, A. X-ray absorption spectroscopy under reaction conditions: suitability of different reaction cells for combined catalyst characterization and time-resolved studies. *Phys. Chem. Chem. Phys.* **2004**, *6*, 3037-3047.

(30)Grunwaldt, J.-D.; Wagner, J. B.; Dunin-Borkowski, R. E. Imaging Catalysts at Work: A Hierarchical Approach from the Macro- to the Meso- and Nano-scale. *Chem. Cat. Chem.* **2013**, *5*, 62-80.

(31)Mutz, B.; Carvalho, H. W. P.; Mangold, S.; Kleist, W.; Grunwaldt, J.-D. Methanation of CO_2: Structural response of a Ni-based catalyst under fluctuating reaction conditions unraveled by operando spectroscopy. *J. Catal.* **2015**, *327*, 48-53.

(32)Grunwaldt, J.-D.; Molenbroek, A. M.; Topsøe, N. Y.; Topsøe, H.; Clausen, B. S. In Situ Investigations of Structural Changes in Cu/ZnO Catalysts. *J. Catal.* **2000**, *194*, 452-460.

(33)Duarte, R. B.; Safonova, O. V.; Krumeich, F.; van Bokhoven, J. A. Atomically dispersed rhodium on a support: the influence of a metal precursor and a support. *Phys. Chem. Chem. Phys.* **2014**, *16*, 26553-26560.

(34)Keresszegi, C.; Grunwaldt, J.-D.; Mallat, T.; Baiker, A. Liquid phase oxidation of alcohols with oxygen: in situ monitoring of the oxidation state of Bi-promoted Pd/Al_2O_3. *Chem. Commun.* **2003**, 2304-2305.

(35)Padmos, J. D.; Personick, M. L.; Tang, Q.; Duchesne, P. N.; Jiang, D.-e.; Mirkin, C. A.; Zhang, P. The surface structure of silver-coated gold nanocrystals and its influence on shape control. *Nat. Commun.* **2015**, *6*, 7664.

(36)Baurecht, D.; Fringeli, U. P. Quantitative modulated excitation Fourier transform infrared spectroscopy. *Rev. Sci. Instrum.* **2001**, *72*, 3782-3792.

(37)Ferri, D.; Newton, M. A.; Nachtegaal, M. Modulation Excitation X-Ray Absorption Spectroscopy to Probe Surface Species on Heterogeneous Catalysts. *Top. Catal.* **2011**, *54*, 1070.

(38)König, C. F. J.; Schildhauer, T. J.; Nachtegaal, M. Methane synthesis and sulfur removal over a Ru catalyst probed in situ with high sensitivity X-ray absorption spectroscopy. *J. Catal.* **2013**, *305*, 92-100.

(39)König, C. F. J.; van Bokhoven, J. A.; Schildhauer, T. J.; Nachtegaal, M. Quantitative Analysis of Modulated Excitation X-ray Absorption Spectra: Enhanced Precision of EXAFS Fitting. *J. Phys. Chem. C* **2012**, *116*, 19857-19866.

(40)Lu, Y.; Keav, S.; Marchionni, V.; Chiarello, G. L.; Pappacena, A.; Di Michiel, M.; Newton, M. A.; Weidenkaff, A.; Ferri, D. Ageing induced improvement of methane oxidation activity of Pd/YFeO3. *Catal. Sci. Tech.* **2014**, *4*, 2919-2931.

(41)Urakawa, A.; Bürgi, T.; Baiker, A. Kinetic analysis using square-wave stimulation in modulation excitation spectroscopy: Mixing property of a flow-through PM-IRRAS cell. *Chem. Phys.* **2006**, *324*, 653-658.

(42)Urakawa, A.; Van Beek, W.; Monrabal-Capilla, M.; Galán-Mascarós, J. R.; Palin, L.; Milanesio, M. Combined, Modulation Enhanced X-ray Powder Diffraction and Raman Spectroscopic Study of Structural Transitions in the Spin Crossover Material $[Fe(Htrz)_2(trz)](BF_4)$. *J. Phys. Chem. C* **2011**, *115*, 1323-1329.

(43)Müller, P.; Hermans, I. Applications of Modulation Excitation Spectroscopy in Heterogeneous Catalysis. *Ind. Eng. Chem. Res.* **2017**, *56*, 1123-1136.

(44)Nilsson, J.; Carlsson, P.-A.; Fouladvand, S.; Martin, N. M.; Gustafson, J.; Newton, M. A.; Lundgren, E.; Grönbeck, H.; Skoglundh, M. Chemistry of Supported Palladium Nanoparticles during Methane Oxidation. *ACS Catal.* **2015**, *5*, 2481-2489.

(45)Chiarello, G. L.; Ferri, D. Modulated excitation extended X-ray absorption fine structure spectroscopy. *Phys. Chem. Chem. Phys.* **2015**, *17*, 10579-10591.

(46)Houssenbay, S.; Payen, E.; Kasztelan, S.; Grimblot, J. Oxidic precursors of molybdena supported on nickel and magnesium aluminate hydrotreating catalysts. *Catal. Today* **1991**, *10*, 541-560.

(47)Furimsky, E. Catalytic hydrodeoxygenation. *Appl. Catal. A* **2000**, *199*, 147-190.

(48)Dabros, T. M. H.; Gaur, A.; Pintos, D. G.; Sprenger, P.; Høj, M.; Hansen, T. W.; Studt, F.; Gabrielsen, J.; Grunwaldt, J.-D.; Jensen, A. D. Influence of H_2O and H_2S on the composition, activity and stability of sulfided Mo, CoMo, and NiMo supported on $MgAl_2O_4$ for hydrodeoxygenation of ethylene glycol. *Appl. Catal. A* **2018**, *551*, 106-121.

(49)Frahm, R. Quick scanning exafs: First experiments. *Nucl. Instrum. Methods Phys. Res. A* **1988**, *270*, 578-581.

(50)Frahm, R. New method for time dependent x-ray absorption studies. *Rev. Sci. Instrum.* **1989**, *60*, 2515-2518.

(51)Müller, O. Hard X-ray Synchrotron Beamline Instrumentation for Millisecond Quick Extended X-ray Absorption Spectroscopy. PhD Dissertation, Bergische Universität Wuppertal, 2016.

(52)Urakawa, A.; Bürgi, T.; Baiker, A. Sensitivity enhancement and dynamic behavior analysis by modulation excitation spectroscopy: Principle and application in heterogeneous catalysis. *Chem. Eng. Sci.* **2008**, *63*, 4902-4909.

(53)Müller, O.; Nachtegaal, M.; Just, J.; Lützenkirchen-Hecht, D.; Frahm, R. Quick-EXAFS setup at the SuperXAS beamline for in situ X-ray absorption spectroscopy with 10 ms time resolution. *J Synchrotron Radiat.* **2016**, *23*, 260-266.

(54)Ravel, B.; Newville, M. ATHENA, ARTEMIS, HEPHAESTUS: data analysis for X-ray absorption spectroscopy using IFEFFIT. *J Synchrotron Radiat.* **2005**, *12*, 537-541.

(55)Kresse, G.; Furthmüller, J. Efficient iterative schemes for ab initio total-energy calculations using a plane-wave basis set. *Phys. Rev. B* **1996**, *54*, 11169-11186.

(56)Kresse, G.; Furthmüller, J. Efficiency of ab-initio total energy calculations for metals and semiconductors using a plane-wave basis set. *Comput. Mat. Sci.* **1996**, *6*, 15-50.

(57)Bahn, S. R.; Jacobsen, K. W. An object-oriented scripting interface to a legacy electronic structure code. *Comput. Sci. Eng.* **2002**, *4*, 56-66.

(58)Wellendorff, J.; Lundgaard, K. T.; Møgelhøj, A.; Petzold, V.; Landis, D. D.; Nørskov, J. K.; Bligaard, T.; Jacobsen, K. W. Density functionals for surface science: Exchange-correlation model development with Bayesian error estimation. *Phys. Rev. B* **2012**, *85*, 235149.

(59)Blöchl, P. E. Projector augmented-wave method. *Phys. Rev. B* **1994**, *50*, 17953-17979.

(60)Kresse, G.; Joubert, D. From ultrasoft pseudopotentials to the projector augmented-wave method. *Phys. Rev. B* **1999**, *59*, 1758-1775.

(61)Tsai, C.; Chan, K.; Abild-Pedersen, F.; Norskov, J. K. Active edge sites in MoSe₂ and WSe₂ catalysts for the hydrogen evolution reaction: a density functional study. *Phys. Chem. Chem. Phys.* **2014**, *16*, 13156-13164.

(62)Tsai, C.; Chan, K.; Norskov, J. K.; Abild-Pedersen, F. Rational design of MoS₂ catalysts: tuning the structure and activity via transition metal doping. *Catal. Sci. Tech.* **2015**, *5*, 246-253.

(63)Moses, P. G.; Hinnemann, B.; Topsøe, H.; Nørskov, J. K. The hydrogenation and direct desulfurization reaction pathway in thiophene hydrodesulfurization over MoS2 catalysts at realistic conditions: A density functional study. *J. Catal.* **2007**, *248*, 188-203.

(64)Monkhorst, H. J.; Pack, J. D. Special points for Brillouin-zone integrations. *Phys. Rev. B* **1976**, *13*, 5188-5192.

(65)Dudarev, S. L.; Botton, G. A.; Savrasov, S. Y.; Humphreys, C. J.; Sutton, A. P. Electron-energy-loss spectra and the structural stability of nickel oxide: An LSDA+U study. *Phy. Rev. B.* **1998**, *57*, 1505-1509.

(66)Rehr, J. J.; Kas, J. J.; Vila, F. D.; Prange, M. P.; Jorissen, K. Parameter-free calculations of X-ray spectra with FEFF9. *Phys. Chem. Chem. Phys.* **2010**, *12*, 5503-5513.

(67)Medici, L.; Prins, R. The Influence of Chelating Ligands on the Sulfidation of Ni and Mo in NiMo/SiO2 Hydrotreating Catalysts. *J. Catal.* **1996**, *163*, 38-49.

(68)van Haandel, L.; Bremmer, G. M.; Hensen, E. J. M.; Weber, T. Influence of sulfiding agent and pressure on structure and performance of CoMo/Al2O3 hydrodesulfurization catalysts. *J. Catal.* **2016**, *342*, 27-39.

(69)Shido, T.; Prins, R. Why EXAFS Underestimated the Size of Small Supported MoS2 Particles. *J. Phys. Chem. B* **1998**, *102*, 8426-8435.
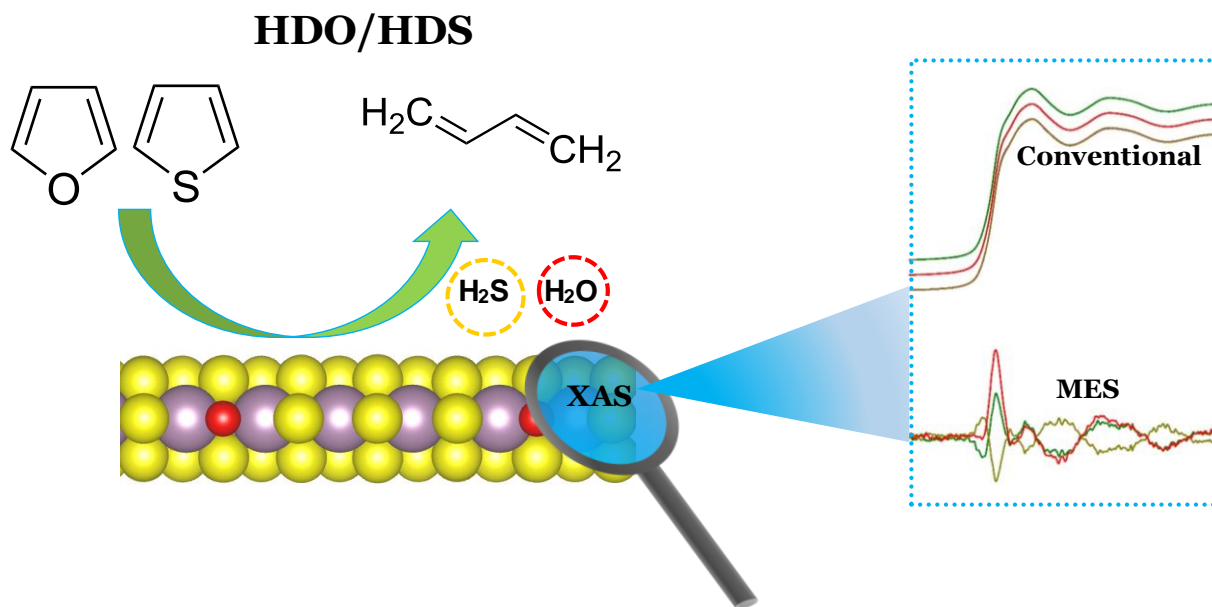
(70)Seo, H.-R.; Lee, Y.-K. EXAFS Studies on the Formation of MoS₂ Nanowires. *J. Korean Phy. Soc.* **2011**, *59*, 730-734.

(71)Jaramillo, T. F.; Jørgensen, K. P.; Bonde, J.; Nielsen, J. H.; Horch, S.; Chorkendorff, I. Identification of Active Edge Sites for Electrochemical H₂ Evolution from MoS2 Nanocatalysts. *Science* **2007**, *317*, 100-102.

(72)Bouwens, S. M. A. M.; Van Veen, J. A. R.; Koningsberger, D. C.; De Beer, V. H. J.; Prins, R. EXAFS determination of the structure of cobalt in carbon-supported cobalt and cobalt-molybdenum sulfide hydrodesulfurization catalysts. *J. Phys. Chem.* **1991**, *95*, 123-134.

(73)Hamabe, Y.; Jung, S.; Suzuki, H.; Koizumi, N.; Yamada, M. Quasi in situ Ni K-edge EXAFS investigation of the spent NiMo catalyst from ultra-deep hydrodesulfurization of gas oil in a commercial plant. *J Synchrotron Radiat.* **2010**, *17*, 530-539.

(74)Badawi, M.; Paul, J.-F.; Cristol, S.; Payen, E. Guaiacol derivatives and inhibiting species adsorption over MoS₂ and CoMoS catalysts under HDO conditions: A DFT study. *Catal. Comm.* **2011**, *12*, 901-905.

Graphical Table of contents